Determination of the Optical Thickness and Effective Particle Radius of Clouds from Reflected Solar Radiation Measurements. Part I: Theory

TERUYUKI NAKAJIMA* AND MICHAEL D. KING

Laboratory for Atmospheres, NASA Goddard Space Flight Center, Greenbelt, Maryland

(Manuscript received 24 August 1989, in final form 1 February 1990)

ABSTRACT

A method is presented for determining the optical thickness and effective particle radius of stratiform cloud layers from reflected solar radiation measurements. A detailed study is presented which shows that the cloud optical thickness (τ_c) and effective particle radius (r_e) of water clouds can be determined solely from reflection function measurements at 0.75 and 2.16 μm, provided $\tau_c \geq 4$ and $r_e \geq 6$ μm. For optically thin clouds the retrieval becomes ambiguous, resulting in two possible solutions for the effective radius and optical thickness. Adding a third channel near 1.65 μm does not improve the situation noticeably, whereas the addition of a channel near 3.70 μm reduces the ambiguity in deriving the effective radius.

The effective radius determined by the above procedure corresponds to the droplet radius at some optical depth within the cloud layer. For clouds having $\tau_c \geq 8$, the effective radius determined using the 0.75 and 2.16 μm channels can be regarded as 85%–95% of the radius at cloud top, which corresponds in turn to an optical depth 20%–40% of the total optical thickness of the cloud layer.

1. Introduction

It is well known that clouds are a strong modulator of the shortwave and longwave components of the earth's radiation budget (Ramanathan 1987; Ramanathan et al. 1989b). In recent years there has been a renewed sensitivity to the importance of clouds and radiation in studies of the earth's climate (Ramanathan et al. 1989a; Cess et al. 1989). It is also now recognized that a knowledge of cloud properties and their variation in space and time is crucial to studies of global climate change (e.g., trace gas greenhouse effects), as general circulation model (GCM) simulations indicate climate-induced changes in cloud amount and vertical structure (Wetherald and Manabe 1988), with a corresponding cloud feedback working to enhance global warming. Recent GCM simulations by Roeckner et al. (1987) and Mitchell et al. (1989) include corresponding changes in liquid water content and cloud optical thickness, and suggest that changes in cloud optical properties may result in a negative feedback comparable in size to the positive feedback associated with changes in cloud cover. None of the GCM simulations to date include corresponding changes in cloud microphysical properties (e.g., particle size), which could easily modify conclusions thus far obtained.

Clouds occur in the earth's atmosphere as a result of the widespread distribution of aerosols, which serve as the primary source of cloud condensation nuclei (CCN). The effect of both natural and anthropogenic aerosols on cloud physics, chemistry, and albedo is an active area of research (Twomey 1980; Hudson 1983). Charlson et al. (1987) argue that the major source of CCN in the marine environment is dimethylsulphide produced by phytoplankton. Furthermore, the possibility exists that the expected increase in anthropogenic aerosol can result in clouds with higher albedos, as Coakley et al. (1987) and Radke et al. (1989) have demonstrated from satellite and in situ aircraft observations of clouds modified by effluents from ships. Twomey et al. (1984) have analyzed the effect of anthropogenic aerosols from continents on cloud albedo and concluded that the loss of sunlight may compensate for the expected warming by CO_2. Wigley (1989) further raised the possibility that the large increase in SO_2 emissions that has occurred in the Northern Hemisphere this century may have resulted in greater sulfate CCN and hence enhanced cooling of the Northern Hemisphere, relative to the Southern Hemisphere. Thus, the simultaneous study of both cloud and aerosol optical properties is of paramount importance to the enhanced understanding of the global climate system.

There are a number of studies of the determination of cloud optical thickness and/or effective particle radius from multiwavelength radiometers from aircraft

* Permanent affiliation: Research Center for Atmospheric and Oceanic Variations, Faculty of Science, Tohoku University, Sendai 980, Japan.

Corresponding author address: Dr. Michael D. King, NASA Goddard Space Flight Center, Code 913, Greenbelt, MD 20771.

(Hansen and Pollack 1970; Twomey and Cocks 1982, 1989; King 1987; Foot 1988) and from satellites (Curran and Wu 1982; Arking and Childs 1985; Rossow et al. 1989). The underlying principle on which these techniques are based is the fact that the reflection function of clouds at a nonabsorbing channel in the visible wavelength region is primarily a function of the cloud optical thickness, whereas the reflection function at a water (or ice) absorbing channel in the near-infrared is primarily a function of cloud particle size. Durkee (1989) performed an empirical study in which he showed a good correlation between the reflection function at 3.7 μm and the effective radius determined from in situ size distribution measurements. Twomey and Cocks (1989) developed a statistical method for simultaneously determining the cloud optical thickness and effective radius using reflected intensity measurements at several wavelengths in the near-infrared region.

Although these studies have demonstrated the applicability of remote sensing methods to the determination of cloud optical and microphysical properties, more theoretical and experimental studies are required in order to assess the soundness and accuracy of these methods when applied to measurements on a global scale. From the theoretical point of view, the recent application of asymptotic theory to the determination of cloud optical thickness (King 1987) has demonstrated the physical basis of the optical thickness retrieval and its efficient implementation to experimental observations. This method is worth incorporating as one component of any multiwavelength algorithm for simultaneously determining the cloud optical thickness and effective radius. From the experimental point of view, more aircraft validation experiments are required in order to assess the validity of these methods, since many factors affect the successful retrieval of these parameters when applied to real data in a real atmosphere (e.g., Rossow et al. 1985; Wu 1985).

The intent of this paper is to present a procedure for inferring the optical thickness and effective particle radius of stratiform cloud layers from multiwavelength reflected solar radiation measurements. This procedure is especially direct and efficient for optically thick layers, where asymptotic expressions for the reflection function are the most valid, but can be applied to the full range of optical thicknesses using interpolation of radiative transfer calculations. It will be demonstrated that the determination of the cloud particle size using reflected solar radiation measurements at 0.75 and 2.16 μm is ambiguous for optically thin layers, where two distinct particle radii and optical thicknesses produce the same reflection functions at these wavelengths. The effect of adding additional channels at 1.65 and 3.70 μm will also be examined, as well as the effect of vertical inhomogeneity on the derivation of effective particle radius.

2. Reflection function of thick atmospheres

When the optical thickness of the atmosphere is sufficiently large, numerical results for the reflection function must agree with known asymptotic expressions for thick layers (van de Hulst 1980). The reflection function $R(\tau_c; \mu, \mu_0, \phi)$ represents the albedo of the medium that would be obtained from a directional reflectance measurement if the reflected radiation field were isotropic. It is formed from a ratio of the reflected intensity $I(0, -\mu, \phi)$ and the incident solar flux density F_0, and is defined by

$$R(\tau_c; \mu, \mu_0, \phi) = \frac{\pi I(0, -\mu, \phi)}{\mu_0 F_0}, \qquad (1)$$

where τ_c is the total optical thickness of the atmosphere (or cloud), μ_0 the cosine of the solar zenith angle, μ the absolute value of the cosine of the zenith angle, measured with respect to the positive τ direction, and ϕ the relative azimuth angle between the direction of propagation of the emerging radiation and incident solar direction.

In the case of optically thick layers overlying a Lambertian surface, the expression for the reflection function of a conservative scattering atmosphere can be written as (King 1987)

$$R(\tau_c; \mu, \mu_0, \phi) = R_\infty(\mu, \mu_0, \phi) - \frac{4(1 - A_g)K(\mu)K(\mu_0)}{[3(1 - A_g)(1 - g)(\tau_c + 2q_0) + 4A_g]}, \qquad (2)$$

from which the scaled optical thickness τ_c' can readily be derived:

$$\tau_c' = (1 - g)\tau_c = \frac{4K(\mu)K(\mu_0)}{3[R_\infty(\mu, \mu_0, \phi) - R(\tau_c; \mu, \mu_0, \phi)]} - 2q' - \frac{4A_g}{3(1 - A_g)}. \qquad (3)$$

In these expressions $R(\tau_c; \mu, \mu_0, \phi)$ is the measured reflection function at a nonabsorbing wavelength, $R_\infty(\mu, \mu_0, \phi)$ the reflection function of a semi-infinite atmosphere, $K(\mu)$ the escape function, A_g the surface (ground) albedo, g the asymmetry factor, and q_0 the extrapolation length for conservative scattering. The reduced extrapolation length $q' = (1 - g)q_0$ lies in the range of 0.709 to 0.715 for all possible phase functions (van de Hulst 1980), and can thus be regarded as a constant ($q' \sim 0.714$).

From Eq. (3) we see that the scaled optical thickness of a cloud depends on q', A_g, $K(\mu)$ and the *difference* between $R_\infty(\mu, \mu_0, \phi)$ and the measured reflection function. This algorithm, first described and applied by King (1987), has been successfully applied to deriving the cloud optical thickness from airborne scan-

ning radiometer measurements at 0.75 μm, a wavelength for which clouds are essentially nonabsorbing.

At water-absorbing wavelengths outside the molecular absorption bands (such as 1.65, 2.16 and 3.70 μm), the reflection function of optically thick atmospheres overlying a Lambertian surface can be expressed as (King 1987)

$$R(\tau_c; \mu, \mu_0, \phi) = R_\infty(\mu, \mu_0, \phi) - \frac{m[(1 - A_g A^*)l - A_g mn^2]K(\mu)K(\mu_0)e^{-2k\tau_c}}{[(1 - A_g A^*)(1 - l^2 e^{-2k\tau_c}) + A_g mn^2 l e^{-2k\tau_c}]}, \quad (4)$$

where k is the diffusion exponent (eigenvalue) describing the attenuation of radiation in the diffusion domain, A^* the spherical albedo of a semi-infinite atmosphere, and m, n and l constants. All five asymptotic constants that appear in this expression [A^*, m, n, l and $k/(1 - g)$] are strongly dependent on the single scattering albedo ω_0, with a somewhat weaker dependence on g. In fact, van de Hulst (1974, 1980) and King (1981) have shown that these constants can be well represented by a function of a similarity parameter s, defined by

$$s = \left(\frac{1 - \omega_0}{1 - \omega_0 g}\right)^{1/2}, \quad (5)$$

where s reduces to $(1 - \omega_0)^{1/2}$ for isotropic scattering and spans the range 0 ($\omega_0 = 1$) to 1 ($\omega_0 = 0$). Similarity relations for the asymptotic constants that arise in Eq. (4) have recently been summarized by King et al. (1990).

Thus asymptotic theory [e.g., Eqs. (2) and (4)] shows that the reflection (and transmission) properties of thick layers depend essentially on two parameters of the atmosphere, τ_c' and s, together with the reflectivity of the underlying surface, A_g. The similarity parameter, in turn, depends primarily on the effective particle radius, defined by (Hansen and Travis 1974)

$$r_e = \int_0^\infty r^3 n(r)dr \Big/ \int_0^\infty r^2 n(r)dr, \quad (6)$$

where $n(r)$ is the particle size distribution and r is the particle radius. In addition to τ_c', s and A_g, the details of the single scattering phase function affect the directional reflectance, and are manifest in the above equations primarily through their influence on $R_\infty(\mu, \mu_0, \phi)$ (King 1987).

Figure 1 illustrates the similarity parameter as a function of wavelength for cloudy air masses containing various values of the effective radius. These computations were performed using Mie theory and the complex refractive indices of liquid water, and include the additional contribution of water vapor. In adding the water vapor contribution we assumed a column loading of water vapor within the cloud of 0.45 g cm^{-2} and a cloud (scattering) optical thickness of 16 at $\lambda = 0.75$

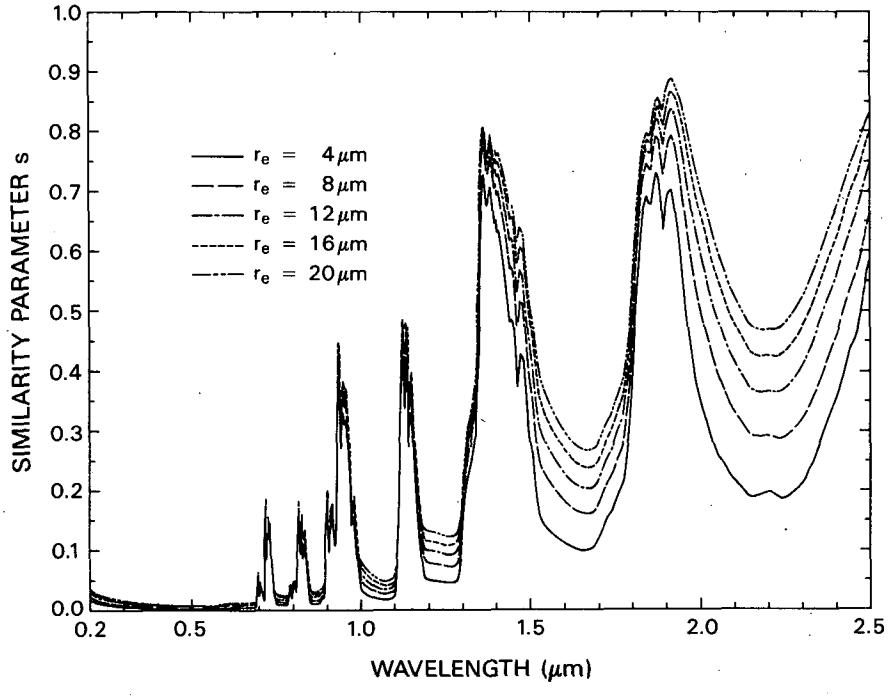

FIG. 1. Cloud similarity parameter as a function of wavelength for selected values of the effective radius. Results apply to water clouds having a modified gamma size distribution with an effective variance $v_e = 0.111$, an optical thickness (at $\lambda = 0.75$ μm) of 16, and saturated water vapor of 0.45 g m^{-2}.

μm (see King et al. 1990 for details). Since the similarity parameter is almost zero (conservative scattering) in the water vapor windows at wavelengths $\lambda \leqslant 1.0$ μm, the cloud optical thickness can be derived primarily from reflection function measurements in this wavelength region [cf. Eq. (3)]. Figure 1 also shows that the similarity parameter, and hence the reflection function, is sensitive to particle size at wavelengths near 1.65 and 2.16 μm, wavelengths for which water vapor absorption is negligible.

The principles outlined above form the basis of methods for simultaneously retrieving the cloud optical thickness and effective radius from multiwavelength reflected solar radiation measurements (Twomey and Seton 1980; Twomey and Cocks 1982, 1989; Curran and Wu 1982). It must be emphasized, however, that the interest in retrieving the optical thickness and effective radius derives not only from the fact that such a retrieval seems possible, but from the fact that cloud radiative properties, especially plane albedo, total transmission, and fractional absorption, depend almost exclusively on these two parameters. This thus forms the basis of cloud radiative parameterization methods, such as the one recently introduced by Slingo (1989), which require that a global database on the effective radius and optical thickness (or equivalently integrated liquid water content) of clouds be available. Such observations seem only to be derivable from spaceborne remote sensing observations.

3. Theoretical background

To assess the sensitivity of the reflection function to cloud optical thickness and effective radius, we performed radiative transfer calculations for a wide variety of solar zenith angles and observational zenith and azimuth angles at selected wavelengths in the visible and near-infrared. Figure 2 shows representative calculations relating the reflection functions at 0.75 and 2.16 μm for various values of τ_c and r_e. These wavelengths were chosen because they are outside the water vapor and oxygen absorption bands and yet have substantially different water droplet (or ice particle) absorption characteristics (cf. Fig. 1). These wavelengths correspond to two channels of the Multispectral Cloud Radiometer (MCR) described by Curran et al. (1981) and King (1987), but may readily be adapted to comparable channels (0.66 and 2.13 μm) of the Moderate Resolution Imaging Spectrometer-Nadir (MODIS-N), to be flown as a NASA facility instrument on the Earth Observing System (Eos) (Salomonson et al. 1989).

The results presented in Fig. 2 correspond to the case when $\mu = 0.883$, $\mu_0 = 0.698$ and $\phi = 63.9°$, a case for which observations were obtained during the marine stratocumulus intensive field observation component of the First ISCCP Regional Experiment (FIRE), conducted off the coast of San Diego during July 1987 (see Albrecht et al. 1988 for a detailed summary of this experiment). These computational results, valid for water clouds, were obtained using the discrete ordinates method for a log-normal distribution of the form

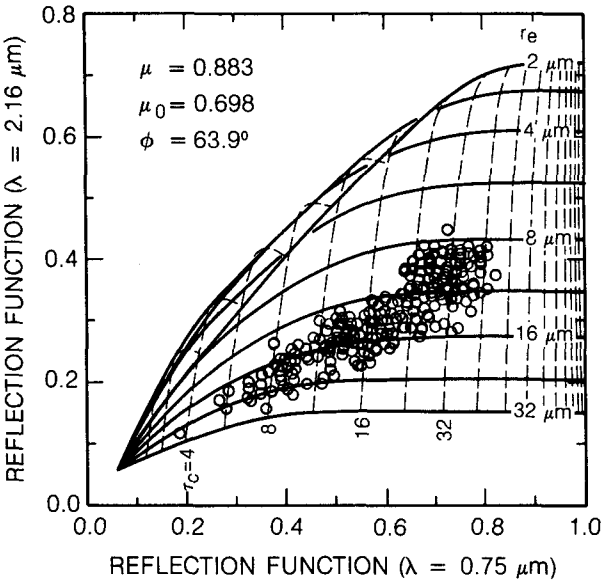

FIG. 2. Theoretical relationships between the reflection function at 0.75 and 2.16 μm for various values of the cloud optical thickness (at $\lambda = 0.75$ μm) and effective particle radius for the case when $\theta_0 = 45.7°$, $\theta = 28.0°$ and $\phi = 63.9°$. Data from measurements above marine stratocumulus clouds during FIRE are superimposed on the figure (10 July 1987).

$$n(r) = \frac{C}{(2\pi)^{1/2}\sigma r} \exp[-(\ln r - \ln r_0)^2/(2\sigma)^2], \quad (7)$$

where r_0 is the mode radius and σ the standard deviation of the cloud droplet size distribution. In terms of these parameters, the effective radius and dimensionless effective variance v_e, defined by (Hansen and Travis 1974)

$$v_e = \int_0^\infty (r - r_e)^2 r^2 n(r) dr \Big/ \int_0^\infty r_e^2 r^2 n(r) dr, \quad (8)$$

may be expressed as

$$r_e = r_0 \exp(5\sigma^2/2), \quad (9)$$

$$v_e = \exp(\sigma^2) - 1. \quad (10)$$

For the results presented in Fig. 2, we assumed $\sigma = 0.35$ ($v_e = 0.13$).

Figure 2 clearly illustrates the underlying principles behind the simultaneous determination of τ_c and r_e from reflected solar radiation measurements. The minimum value of the reflection function at each wavelength corresponds to the reflection function of the underlying surface at that wavelength in the absence of an atmosphere. For the computations presented in

Fig. 2, the underlying surface was assumed to be Lambertian with $A_g = 0.06$, roughly corresponding to an ocean surface. The dashed curves in Fig. 2 represent the reflection functions at 0.75 and 2.16 μm that result for specified values of the cloud optical thickness at 0.75 μm. The solid curves, on the other hand, represent the reflection functions that result for specified values of the effective particle radius. These results show, for example, that the cloud optical thickness is largely determined by the reflection function at a nonabsorbing wavelength (0.75 μm in this case), with little dependence on droplet radius. The reflection function at 2.16 μm, in contrast, is largely sensitive to r_e, with the largest values of the reflection function occurring for small particle sizes. In fact, as the optical thickness increases ($\tau_c \geq 12$), the sensitivity of the nonabsorbing and absorbing channels to τ_c (0.75 μm) and r_e is very nearly orthogonal. This implies that under these optically thick conditions we can determine the optical thickness and effective radius nearly independently, and thus measurement errors in one channel have little impact on the cloud optical property determined primarily by the other channel. Figures similar to Fig. 2 can also be found in Curran and Wu (1982) and Wielicki et al. (1990), who further considered the reflectance properties of ice clouds as well as water clouds.

The data points superimposed on the theoretical curves of Fig. 2 represent measurements obtained with the MCR, a 7-channel scanning radiometer that was mounted in the left wing superpod of the NASA ER-2 aircraft during FIRE. These observations were obtained as the aircraft flew a 145 km flight leg above an extensive stratocumulus cloud layer approximately 350 km offshore on 10 July 1987. A detailed analysis of these and other aircraft observations will be the subject of Part II of this paper. From the measurements presented in Fig. 2, however, one readily draws the conclusion that the optical thickness at $\lambda = 0.75$ μm ranges between 6 and 45 while the effective radius ranges between 8 and 22 μm, and that the effective radius decreases as the optical thickness increases.

Whether one formulates the retrieval of r_e in terms of a ratio of the reflection function at a strongly absorbing channel to a weakly absorbing channel, as in Foot (1988) and Twomey and Cocks (1989), or as an absolute reflection function as in Curran and Wu (1982) and Fig. 2, the underlying principle behind the simultaneous determination of optical thickness and effective radius remains the same. As the effective radius increases, absorption monotonically increases for all $r_e \geq 1.0$ μm. This is illustrated in Fig. 3 where we present computational results of the similarity parameter and asymmetry factor as a function of effective radius for $\lambda = 2.16$ μm and for various values of the standard deviation (or equivalently effective variance) of a log-normal size distribution. For $r_e \geq 1.0$ μm the similarity parameter varies in direct proportion to $r_e^{1/2}$, as suggested by Twomey and Bohren (1980),

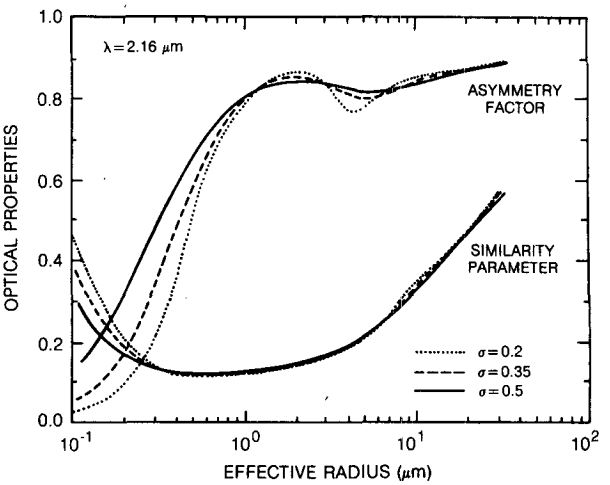

FIG. 3. Similarity parameter and asymmetry factor as a function of effective radius for log-normal distributions of water particles having standard deviations $\sigma = 0.2$, 0.35 and 0.5. Results apply at $\lambda = 2.16$ μm.

with little sensitivity to the variance of the size distribution, in accord with the findings of Curran and Wu (1982). As a consequence of the weak sensitivity of the similarity parameter and asymmetry factor to the dispersion in the size distribution, we have chosen to fix $\sigma = 0.35$ ($v_e = 0.13$) for determining r_e from spectral reflection function measurements.

A striking and unexpected feature of Fig. 2 is the fact that multiple solutions of τ_c (0.75 μm) and r_e are possible from simultaneous reflection function measurements at 0.75 and 2.16 μm, a feature which becomes increasingly pronounced as r_e and τ_c decrease. Figure 2 also shows that the maximum reflection function at 2.16 μm generally occurs for an effective radius between 2 and 4 μm, depending on optical thickness. Since the similarity parameter monotonically increases as the particle radius increases throughout the entire range $r_e \geq 1$ μm (cf. Fig. 3), the explanation for the maximum reflection function at $2 \leq r_e \leq 4$ μm cannot lie in the absorption characteristics alone.

The explanation for this phenomenon may be understood by referring to Fig. 4, which shows the radius sensitivity of the scaled optical thickness at 1.65, 2.16, and 3.70 μm, relative to the scaled optical thickness at 0.75 μm. The scaled optical thickness was selected because the reflection function at 0.75 μm is primarily a function of scaled optical thickness, in terms of which the dashed lines in Fig. 2 would be more nearly vertical [cf. Eqs. (2) and (3)]. The computations presented in Fig. 4 clearly show that the scaled optical thickness at selected water-absorbing wavelengths in the near-infrared reaches a maximum, relative to the scaled optical thickness at 0.75 μm, near a radius $r_e \approx 5$ μm. Thus, the combination of the maximum scaled optical thickness τ_c' (2.16 μm) at $r_e \approx 5$ μm, together with the minimum absorption at $r_e \approx 1$ μm, leads to the max-

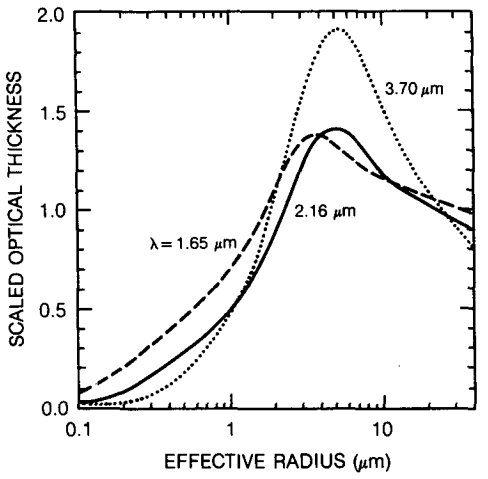

FIG. 4. Ratio of the scaled optical thickness at $\lambda = 1.65$, 2.16 and 3.70 μm to that at $\lambda = 0.75$ μm as a function of effective radius.

imum reflection function at 2.16 μm being achieved for radii between 1 and 5 μm, depending on optical thickness. The multivalued solutions of Fig. 2 thus result from the fact that the similarity parameter *and* scaled optical thickness at $\lambda = 2.16$ μm vary as r_e varies for a fixed value of the reflection function, and hence scaled optical thickness, at 0.75 μm.

In order to help clarify these points, we have computed the spherical albedo as a function of effective radius and scaled optical thickness τ_c' (0.75 μm) for wavelengths of 2.16 and 3.70 μm. These results, presented in Fig. 5, show that the spherical albedo is a peaked function of particle radius, with the radius having the maximum spherical albedo decreasing as the optical thickness increases. Even at $\lambda = 3.70$ μm, which has a much larger absorption than 2.16 μm, the effect of the reduced optical thickness at sizes below $r_e = 5$ μm is significant at $\tau_c' = 4$ ($\tau_c \approx 19$). Since the spherical albedo describes an angular mean feature of the reflection function, the reflection function itself must have a similar sensitivity to particle size. This is consistent with the results presented in Fig. 2, which show that the maximum reflection function at 2.16 μm occurs for a smaller (larger) particle radius the larger (smaller) the optical thickness.

Although the peaked, multivalued feature of the reflection function is to be expected from the results presented in Figs. 4 and 5, the details are dependent on the solar and observational zenith and azimuth angles. Figure 6 illustrates the reflection function at 0.75 and 2.16 μm as a function of effective radius for three different azimuthal angles ($\phi = 0°$, 90° and 180°) when the solar zenith angle $\theta_0 = 60°$ and the emergent zenith angle $\theta = 50°$. From these results we conclude that the optical thickness retrieval, which depends primarily on $\lambda = 0.75$ μm, does not depend strongly on effective radius unless the particles become small and the azimuth angle approaches 180°. Likewise, the reflection function at 2.16 μm is almost independent of the optical thickness, as expected from Fig. 2, such that the particle radius is determined uniquely from reflection function measurements at 2.16 μm, unless ϕ approaches 180°. Near $\phi = 180°$, the reflection function has a peak at $r_e \approx 5$ μm which corresponds to the multivalued function discussed above. Although the location of this peak depends on scattering angle, the general origin of this feature arises from the fact that particles loose their scattering efficiency faster for longer wavelengths as the particle radius decreases.

4. Determination of the cloud optical thickness and effective radius

From the principles outlined above, we conclude that the greatest sensitivity of the reflection function

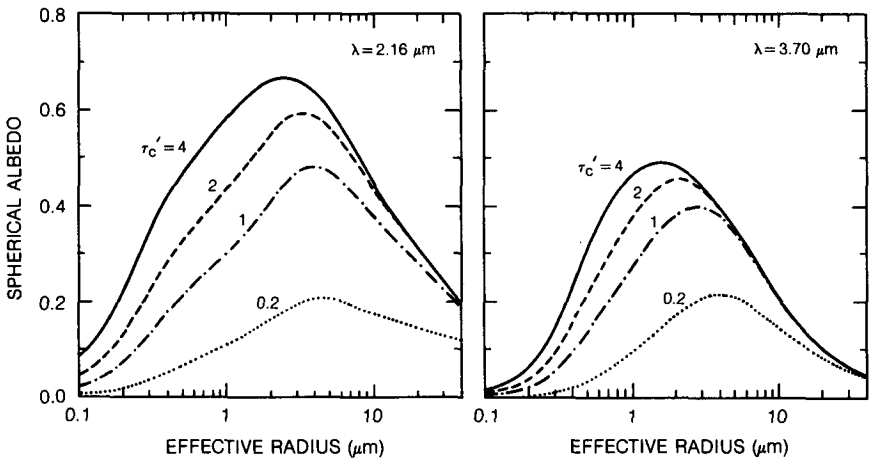

FIG. 5. Spherical albedo as a function of effective radius for four values of the scaled optical thickness at $\lambda = 0.75$ μm. The panel on the left applies to computations at $\lambda = 2.16$ μm and the panel on the right to 3.70 μm.

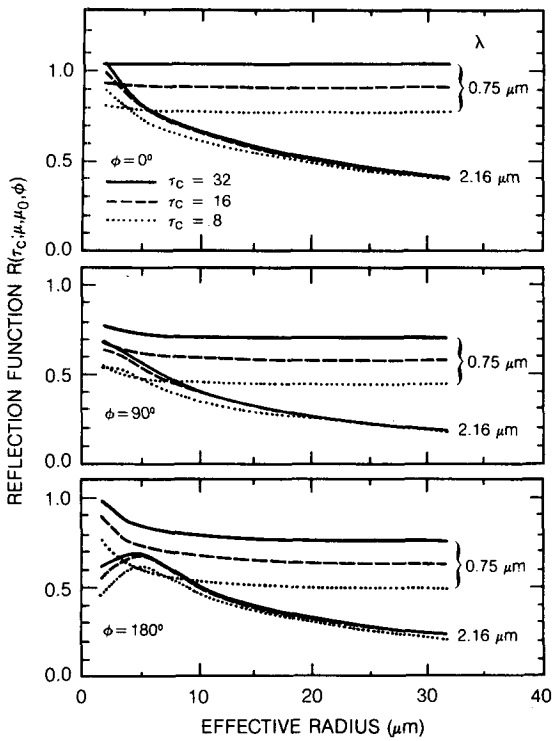

FIG. 6. Reflection function as a function of effective radius for $\theta_0 = 60°$, $\theta = 50°$, and for different values of azimuth angle, wavelength and cloud optical thickness at 0.75 μm.

to cloud optical thickness occurs for conservative scattering when the underlying surface albedo is small. Likewise, the largest sensitivity of the reflection function to effective radius occurs for nonconservative scattering near 1.65, 2.16 and 3.70 μm. Figure 7 illustrates computations of the spherical albedo as a function of τ_c (0.75 μm) and r_e for 0.75 μm (solid curves) and 2.16 μm (dashed curves). These results are analogous to Fig. 2 but with a remapping of the orthogonal axes to τ_c (0.75 μm) and r_e. In terms of scaled optical thickness the solid curves in Fig. 7 would be nearly horizontal, as predicted by the spherical albedo equivalent of Eq. (1). The additional information provided by a simultaneous measurement at 2.16 μm permits the effective radius, and hence asymmetry factor, to be determined, thereby enabling τ_c (0.75 μm) to be derived.

Figure 7 shows, once again, that reflectance measurements at 0.75 and 2.16 μm are nearly orthogonal for optically thick layers. This figure also demonstrates that reflectance measurements at 0.75 μm are important for determining the effective radius and optical thickness when the particles are small. For optically thin atmospheres with submicron particle sizes, reflectance measurements at 0.75 and 2.16 μm are seen to be orthogonal as well, suggesting that the simultaneous use of reflection function measurements at these, or similar, wavelengths may be utilized to retrieve corresponding aerosol properties.

If one assumes that each reflection function measurement is made with equal relative precision, maximizing the probability that $R^i_{\text{meas}}(\mu, \mu_0, \phi)$ observations have the functional form $R^i_{\text{calc}}(\tau_c, r_e; \mu, \mu_0, \phi)$ is equivalent to minimizing the statistic χ^2, defined as

$$\chi^2 = \sum_i [\ln R^i_{\text{meas}}(\mu, \mu_0, \phi) - \ln R^i_{\text{calc}}(\tau_c, r_e; \mu, \mu_0, \phi)]^2, \quad (11)$$

where the summation extends over all wavelengths λ_i for which measurements have been made and calculations performed. Twomey and Cocks (1989) adopted an alternative formulation to this expression which represents a more complicated weighting of the spectral reflection function measurements. It seems unlikely that significantly different solutions for τ_c (0.75 μm) and r_e would result from the application of these alternative formulations.

Minimizing χ^2 as defined by (11) is equivalent to making an unweighted least-squares fit to the data (Bevington 1969). The minimum value of χ^2 can be determined by setting the partial derivatives of χ^2 with respect to each of the coefficients [τ_c (0.75 μm), r_e] equal to zero. Due to the complicated dependence of the reflection functions on τ_c and r_e, however, this solution is nonlinear in the unknowns τ_c and r_e such that no analytic solution for the coefficients exists. Even for optically thick layers, where asymptotic theory applies, $R^i_\infty(r_e; \mu, \mu_0, \phi)$ is a complicated function of the phase function, and hence r_e, as King (1987) has shown by deriving the cloud optical thickness assuming the clouds had two different phase functions but the same asymmetry factor.

In order to solve this nonlinear least-squares problem, we have adopted a procedure whereby the scaled

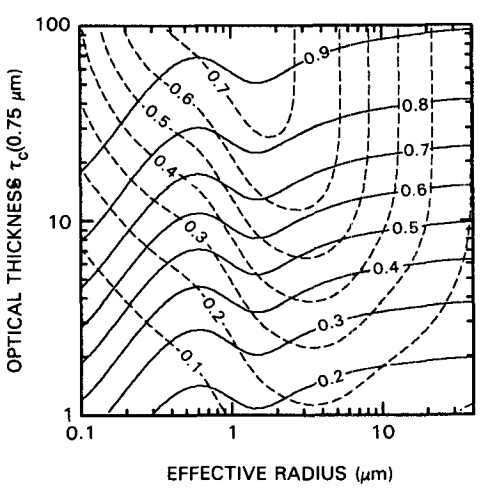

FIG. 7. Spherical albedo as a function of τ_c (0.75 μm) and r_e for λ = 0.75 μm (solid curves) and 2.16 μm (dashed curves).

optical thickness $\tau_c'(0.75\ \mu m)$, and hence $\tau_c(0.75\ \mu m)$ and g, is determined as a function of r_e from a reflection function measurement at 0.75 μm (cf. Fig. 7). For $\tau_c' < 1.8$ we used spline under tension interpolation (Cline 1974) of reflection function calculations $R^i_{calc}(\tau_c, r_e; \mu, \mu_0, \phi)$, and for $\tau_c' \geq 1.8$ we used Eq. (3), as described by King (1987). Having determined an array of possible solutions $[\tau_c(0.75\ \mu m), r_e]$, it is straightforward to calculate χ^2 as a function of r_e using measurements and calculations for one or more additional channels. Thus, the determination of the optimum values of $\tau_c(0.75\ \mu m)$ and r_e becomes a nonlinear least-squares problem in only one unknown r_e, since $\tau_c(0.75\ \mu m)$ is given uniquely from a knowledge of r_e. The only subtlety worth noting is that it is essential to allow for the spectral dependence of $\tau_c(\lambda)$ and $A_g(\lambda)$ when interpolating radiative transfer calculations $[\tau_c'(\lambda) < 1.8]$ or applying Eq. (4) $[\tau_c'(\lambda) \geq 1.8]$ at channels other than 0.75 μm.

As an illustration of how this procedure works, we have constructed the χ^2 hypersurface in coefficient space for various combinations of channels. These results, presented in Fig. 8, are based on simulated spherical albedo measurements at (a) 0.75 and 2.16 μm, (b) 0.75, 1.65 and 2.16 μm, (c) 0.75 and 3.70 μm, and (d) 0.75, 1.65, 2.16 and 3.70 μm. The solid curves represent constant values of χ^2. The parameters τ_c (0.75 μm) and r_e which give the best fit of the measurements R^i_{meas} to the nonlinear function $R^i_{calc}(\tau_c, r_e)$ are determined by the location of the minimum value of χ^2 in this two-dimensional space. The results presented in Fig. 8 were constructed for the optimum values τ_c (0.75 μm) = 8 and r_e = 6 μm. Searching this hypersurface for the parameters which minimize χ^2 is greatly facilitated by first solving for $\tau_c(0.75\ \mu m)$ as a function of r_e using the reflection function measurement at 0.75 μm. These optical thickness values, shown in each panel of Fig. 8 as a dashed line, must necessarily pass through the absolute minimum of the function χ^2.

From the results presented in Fig. 8, we see that the χ^2 hypersurface frequently has two minima, regardless of the number of channels, with the larger radius so-

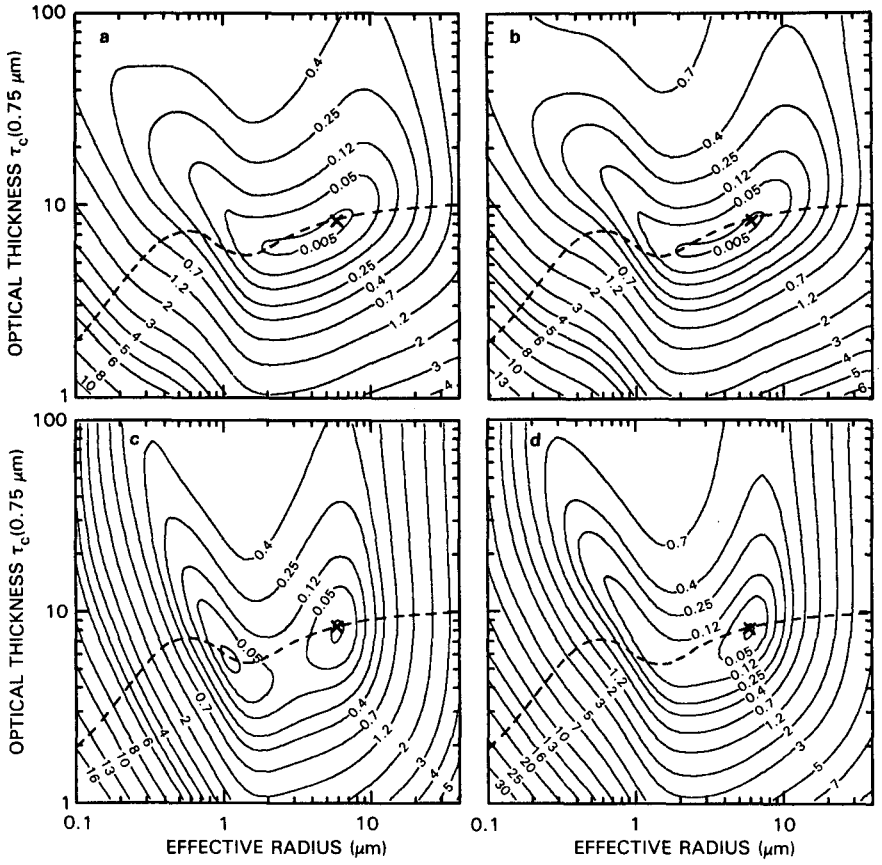

FIG. 8. The χ^2 hypersurface for theoretically generated spherical albedo measurements at (a) 0.75 and 2.16 μm, (b) 0.75, 1.65 and 2.16 μm, (c) 0.75 and 3.70 μm, and (d) 0.75, 1.65, 2.16 and 3.70 μm. The solid curves represent constant values of χ^2, while the dashed curve in each figure represents the array of possible solutions for $R^{0.75}_{meas} = 0.495$ (cf. Fig. 7). These results were constructed for a model cloud layer having τ_c (0.75 μm) = 8 and r_e = 6 μm, located by the minimum value of χ^2 in this two-dimensional space.

lution generally corresponding to cloud particle sizes normally found in terrestrial water clouds. Furthermore, comparison of Figs. 8a and 8b suggests that the introduction of a third channel at 1.65 μm is unnecessary, at least for water clouds, since no substantial improvement in the derivation of $\tau_c(0.75\ \mu\text{m})$ and r_e results from the introduction of an additional channel. This is a direct consequence of the fact that the shape of the χ^2 hypersurface is virtually unchanged in the vicinity of the absolute minimum. At 3.70 μm, where the imaginary part of the complex refractive index is ten times greater than at 2.16 μm, the multivalued solution is even more striking (cf. Figs. 8a and 8c). For our model cloud with $\tau_c(0.75\ \mu\text{m}) = 8$, Fig. 8c shows that a secondary minimum of χ^2 occurs at $r_e \approx 1$ μm and $\tau_c(0.75\ \mu\text{m}) \approx 6$. Since the shape of the contour lines around the minimum is different in Figs. 8a and 8c, a combined use of 2.16 and 3.70 μm helps remove the fictitious solution, as indicated in Fig. 8d. In a practical sense, however, we have found it sufficient to use reflection function measurements solely at 0.75 and 2.16 μm, and to set a reasonable lower limit for an acceptable effective radius. This necessarily forces the algorithm to select the larger of the two possible radii (and optical thickness) solutions.

In order to implement the procedure outlined above, we have computed the reflection function for the standard problem of plane-parallel homogeneous cloud layers with $\tau_c' = 0.4$, 0.8, 1.2 and ∞ and $r_e = 2^{(n+1)/2}$ for $n = 1, \cdots, 9$, assuming a log-normal size distribution with $\sigma = 0.35$. These values of τ_c' were selected such that interpolation errors are everywhere $\leqslant 3\%$ for $\tau_c' \geqslant 0.6$. This was accomplished using a combination of asymptotic theory for $\tau_c' \geqslant 1.8$ and spline under tension interpolation for $\tau_c' < 1.8$. Calculations of the reflection function were performed using the discrete ordinates method with the TM-method of truncating the phase function (Nakajima and Tanaka 1988). The asymptotic functions and constants that appear in (2)–(4) were obtained from solutions of an eigenvalue equation that arises in the discrete ordinates method. Finally, it should be noted that we have neglected the small contributions of molecular scattering and absorption in the above calculations, but will include the effects of water vapor absorption above the cloud and the finite bandwidth of the channels in our airborne radiometer when analyzing data to be presented in Part II.

5. Error analysis

Having determined the cloud optical thickness and effective radius, it is important to examine the overall uncertainties in $\tau_c(0.75\ \mu\text{m})$ and r_e. As discussed extensively by King (1987), these uncertainties arise as a result of errors in the measured reflection function at wavelengths $\lambda_i(\Delta R^i_{\text{meas}})$, as well as uncertainties in the surface albedo, phase function and similarity parameter. Due to the multiwavelength nature of our retrieval algorithm, together with the near orthogonality of the retrieval of $\tau_c(0.75\ \mu\text{m})$ and r_e (cf. Figs. 2 and 7), we have found it particularly useful to examine the errors in τ_c (0.75 μm) arising from uncertainties $\Delta R^{0.75}_{\text{meas}}$, and errors in r_e arising from uncertainties $\Delta R^{2.16}_{\text{meas}}$. Thus we define

$$E_{\tau_c} = 5 \times \frac{\partial \ln \tau_c(0.75\ \mu\text{m})}{\partial \ln R^{0.75}_{\text{meas}}}, \tag{12}$$

$$E_{r_e} = 5 \times \frac{\partial \ln r_e}{\partial \ln R^{2.16}_{\text{meas}}}, \tag{13}$$

which represent, in turn, the percentage error in the optical thickness arising from a 5% error in the measured reflection function at 0.75 μm, and percentage error in the effective radius arising from a 5% error in the measured reflection function at 2.16 μm.

Figure 9 illustrates E_{τ_c} and E_{r_e} as a function of τ_c (0.75 μm) and r_e for the spherical albedo, where the left portion of the figure applies to E_{τ_c} and the right portion to E_{r_e}. Since these computational results apply to the spherical albedo, rather than to the reflection function at specific values of μ, μ_0 and ϕ, these errors represent mean values over a wide range of angles. In general, the errors in the retrieved optical thickness and effective radius are smaller (larger) for small (large) solar zenith angles and forward (backward) scattering. The relative error in the retrieved optical thickness is seen to monotonically increase as the optical thickness increases, exceeding 50% at $\tau_c(0.75\ \mu\text{m}) \approx 50$. This error, which is not a strong function of effective radius, represents the error in $\tau_c(0.75\ \mu\text{m})$ arising solely from an error in $R^{0.75}_{\text{meas}}$. For cases where $r_e \leqslant 4$ μm, errors in the reflection function at other wavelengths also contribute to the uncertainty in $\tau_c(0.75\ \mu\text{m})$. The relative error in the retrieved effective radius E_{r_e}, in contrast to E_{τ_c}, is seen to be a strong function of particle radius, with a much weaker dependence on the cloud optical thickness. This is to be expected from the results presented in Figs. 2 and 7. Furthermore, Fig. 9 shows that E_{r_e} contains a narrow ridge with errors in excess of 100% running from small to large optical thicknesses when r_e is in the range $1 \leqslant r_e \leqslant 4$ μm. On both sides of this ridge the error rapidly decreases to less than 20% for a 5% uncertainty in $R^{2.16}_{\text{meas}}$. Errors in r_e may also result from uncertainties $\Delta R^{0.75}_{\text{meas}}$, even in the absence of any uncertainty $\Delta R^{2.16}_{\text{meas}}$, but this uncertainty leads primarily to uncertainty in selecting the correct radius among the two possible radius solutions.

In order to assess the overall uncertainties in the retrieved optical thickness and effective radius, we performed radiative transfer computations at 0.75, 1.65 and 2.16 μm. At each wavelength the reflection function was computed for $\theta_0 = 10°, 60°$, $\theta = 0°, 10°, 30°, 50°$, $\phi = 0°, 10°, 30°, 60°, 120°, 150°, 170°, 180°$, τ_c (0.75 μm) = 4, 8, 16, 32 and r_e = 4, 8, 16 μm. After

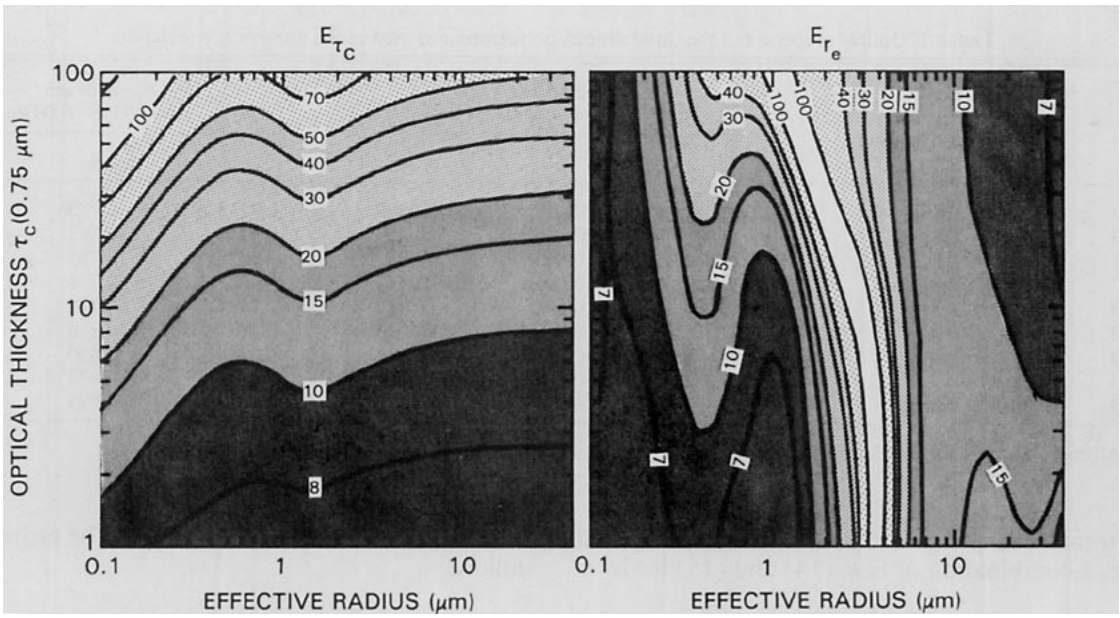

FIG. 9. Relative error in the cloud optical thickness for 5% error in the measured reflection function at 0.75 μm (left panel), and relative error in the effective particle radius for 5% error in the measured reflection function at 2.16 μm (right panel). These results apply to the spherical albedo, and would be somewhat reduced for small solar zenith angles and somewhat enhanced for large solar zenith angles.

confirming that the algorithm returns the correct values of τ_c (0.75 μm) and r_e for simulated measurements with no observational error, we introduced observational error of 5% into the reflection function at one channel, with no observational error in either of the other two channels.

The results of these simulations are presented in Fig. 10, which shows the relationship between errors in r_e and τ_c (0.75 μm) for 5% error in the reflection function at 0.75 μm (solid circles), 1.65 μm (open squares) and 2.16 μm (solid triangles). While there are instances for which the error in τ_c (0.75 μm) is large when the error in r_e is negligible, the overall tendency of these simulations is for an error in τ_c (0.75 μm) to occur whenever there is an error in r_e. The former condition corresponds to the situation in which the optical thickness is large and measurement (or calibration) errors are confined solely to 0.75 μm. The latter condition, on the other hand, occurs primarily when measurement errors occur at 1.65 or 2.16 μm with no corresponding errors at 0.75 μm. These results may be understood as follows. For optically thick layers the reflection function at a nonabsorbing wavelength is primarily a function of the scaled optical thickness [cf. Eq. (2)], and thus the scaled optical thickness retrieved by our analysis is nearly independent of particle radius. Thus,

$$\frac{\partial \ln \tau_c'(0.75\ \mu\text{m})}{\partial \ln r_e} = \frac{\partial \ln(1-g)}{\partial \ln r_e} + \frac{\partial \ln \tau_c(0.75\ \mu\text{m})}{\partial \ln r_e} \approx 0. \quad (14)$$

From computations of the asymmetry factor as a function of effective radius, (Table 1), it follows that at 0.75 μm,

$$\frac{\partial \ln(1-g)}{\partial \ln r_e} \approx -0.50 + 0.15 \ln r_e. \quad (15)$$

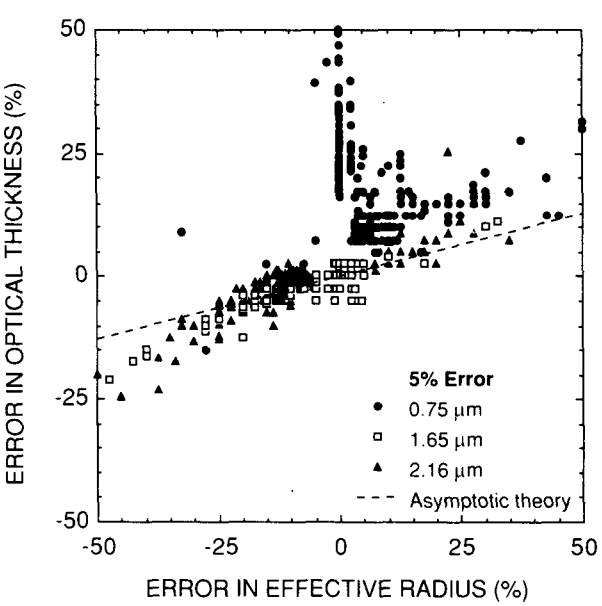

FIG. 10. Simultaneous errors in the retrieved optical thickness and effective radius for simulations containing 5% error in the reflection function at 0.75 μm (solid circles), 1.65 μm (open squares) or 2.16 μm (solid triangles). The dashed curve superimposed on these results is the error predicted by Eq. (16) (see text for details).

TABLE 1. Optical properties of the cloud droplet polydispersions used in the numerical simulations.*

	$\lambda = 0.75\ \mu m$ $m = 1.332 - 0.0i$	$\lambda = 2.16\ \mu m$ $m = 1.294 - 0.00035i$			$\lambda = 3.70\ \mu m$ $m = 1.374 - 0.0036i$		
r_e	g	ω_0	g	k	ω_0	g	k
2.13	0.782	0.99708	0.853	0.0360	0.9783	0.790	0.119
3.00	0.812	0.99578	0.836	0.0458	0.9747	0.802	0.125
4.25	0.832	0.99288	0.803	0.0652	0.9627	0.783	0.160
6.00	0.846	0.98880	0.801	0.0824	0.9387	0.756	0.217
8.50	0.856	0.98408	0.828	0.0917	0.9099	0.775	0.256
12.00	0.862	0.97786	0.850	0.1019	0.8811	0.819	0.275
17.00	0.867	0.96949	0.863	0.1160	0.8465	0.850	0.302
24.00	0.870	0.95849	0.874	0.1321	0.8045	0.872	0.336
34.00	0.873	0.94398	0.885	0.1508	0.7558	0.893	0.375

* All computations were performed assuming the log-normal size distribution with $\sigma = 0.35$ ($v_e = 0.13$).

In the radius range $4 \leqslant r_e \leqslant 6\ \mu m$, where E_{r_e} is especially large, a combination of Eqs. (14) and (15) leads to

$$\frac{\partial \ln \tau_c (0.75\ \mu m)}{\partial \ln r_e} \approx 0.26. \tag{16}$$

This result, shown in Fig. 10 as a dashed line, is seen to be a reasonable approximation for $|\Delta r_e / r_e| \leqslant 25\%$ and for cases in which the measurement error is confined largely to 1.65 or 2.16 μm. The large errors in droplet radius, which are generally associated with errors in excess of those predicted by (16), arise primarily when τ_c (0.75 μm) and r_e are small, cases for which asymptotic theory and the assumption of (14) are no longer valid. In a one-channel method for determining the cloud optical thickness (cf. King 1987; Rossow et al. 1989), where it is necessary to assume a value of r_e, Fig. 10 suggests that errors of ±25% can arise in the optical thickness for errors of ±50% in effective radius.

6. Effect of inhomogeneous vertical stratification

In the preceding sections we examined the possibility of determining τ_c (0.75 μm) and r_e for the ideal situation in which the cloud layer is plane parallel and vertically homogeneous. Since terrestrial water clouds contain significant vertical inhomogeneity, it is important to examine the effect this vertical stratification has on reflected solar radiation measurements. Many investigations have shown that cloud liquid water content w and effective radius r_e are linearly increasing functions of height z, with the exception of the uppermost optically thin entrainment region. Thus, we can write

$$w(z) \approx Az + B, \tag{17}$$

and

$$r_e(z) \approx az + b. \tag{18}$$

Assuming the extinction efficiency factor equals 2, the cloud optical thickness at level z can be estimated as follows:

$$\tau \approx \frac{3}{2\rho} \int_z^{z_t} \frac{w(z')}{r_e(z')}\, dz'$$

$$\approx \frac{3Ar_t}{2\rho a^2} \left(1 - \hat{r} + \frac{w_t \hat{r}_b - w_b}{w_t - w_b} \ln \hat{r} \right), \tag{19}$$

where ρ is the density of water, w_t and w_b the liquid water contents at the cloud top and cloud base, respectively, r_t and r_b the effective radii at the cloud top and cloud base, and $\hat{r}$ the normalized effective radius defined by

$$\hat{r} = r_e(z)/r_t. \tag{20}$$

Assuming $w_b = 0$ at cloud base, the normalized optical depth,

$$\hat{\tau} = \frac{\tau}{\tau_c} \approx \frac{1 - \hat{r} + \hat{r}_b \ln \hat{r}}{1 - \hat{r}_b + \hat{r}_b \ln \hat{r}_b}, \tag{21}$$

does not depend on the vertical profile of cloud liquid water content and is determined solely by the normalized effective radius at cloud base $\hat{r}_b$.

Since $\hat{r}_b$ is not a strongly varying parameter for marine stratocumulus clouds, the normalized optical depth $\hat{\tau}$ defined by (21) is expected to follow very nearly a unique function of $\hat{r}$. For example, $\hat{r}_b$ ranges between 0.49 and 0.58 for the in situ microphysical measurements presented by Slingo et al. (1982), Stephens and Platt (1987), Albrecht et al. (1988) and Spinhirne et al. (1989). Figure 11 illustrates profiles of $\hat{r}$ as a function of $\hat{\tau}$ determined from these results. Although the optical thickness in these cases ranges between 6 and 21, the normalized vertical profiles of effective radius are quite similar for all four cases. Thus we have adopted the profile given by (21) with $\hat{r}_b = 0.57$, corresponding to Albrecht et al.'s (1988) results obtained off the coast of southern California during FIRE. This profile of effective radius as a function of optical depth

can thus be regarded as a suitable model of vertical inhomogeneity for marine stratocumulus clouds. These results show, for example, that approximately 70% of the cloud optical thickness lies above the geometric midlevel of the cloud, a level for which $\hat{r} \approx 0.5(1 + \hat{r}_b)$.

In order to examine the effect of inhomogeneous vertical stratification, we performed numerical simulations of the reflection function for two of the vertically inhomogeneous models shown in Fig. 11. In addition to the Albrecht et al. (1988) model for marine stratocumulus clouds, which we will refer to as model A, we simulated the radiative properties of an inhomogeneous cloud layer having the extreme vertical inhomogeneity represented by the dashed line in Fig. 11 (model B). For each of these vertically inhomogeneous cloud models we computed the reflection function at 0.75, 1.65 and 2.16 μm for $\theta_0 = 0°, 60°$, $\theta = 0°, 30°, 50°$, $\phi = 0°, 30°, 60°, 120°, 150°, 180°$, $\tau_c(0.75\ \mu\text{m}) = 4, 8, 16, 32$ and $r_t = 4, 6, 8, 12, 16\ \mu$m. These simulated reflection function measurements were then used to retrieve $\tau_c(0.75\ \mu\text{m})$ and r_e using our operational retrieval algorithm based on a vertically homogeneous atmosphere, as described in section 4.

The effective radius retrieved from our analysis necessarily represents some mean, or equivalent, effective radius r_{remote}. This remote sensing-derived radius can be regarded as the effective radius at an equivalent optical depth τ_{eq} within the cloud layer such that the spectral reflection function of the vertically inhomogeneous cloud is similar to that of a homogeneous cloud layer having an optical thickness $\tau_c(0.75\ \mu\text{m}) = \tau_{\text{remote}}$ and effective radius $r_e = r_{\text{remote}}$. Thus we can write:

$$\hat{\tau}_{\text{eq}} = \frac{\tau_{\text{eq}}}{\tau_c} = \hat{\tau}(\hat{r}_{\text{remote}}), \tag{22}$$

where

$$\hat{r}_{\text{remote}} = r_{\text{remote}}/r_t. \tag{23}$$

Figure 12a illustrates $\tau_{\text{remote}}/\tau_c$ as a function of r_t and τ_c for models A and B, where τ_c represents the true optical thickness of the cloud layer. These results show that our remote sensing method tends to overestimate the true cloud optical thickness, and that the overestimate decreases as r_t increases and the vertical inhomogeneity decreases (model A is less inhomogeneous than model B). Furthermore, when $r_t = 4\ \mu$m, an unrealistically small value for terrestrial water clouds, τ_{remote} can be overestimated by as much as 33% when $\tau_c = 4$, decreasing as τ_c increases. When $r_t \geq 6\ \mu$m and inhomogeneous model A applies, the cloud optical thickness is overestimated by no more than 3%. The vertical error bars illustrated in Fig. 12a, shown displaced to the left of their corresponding values of r_t, represent standard deviations of $\tau_{\text{remote}}/\tau_c$ obtained for the full range of observational angles, and apply specifically to model A when $\tau_c = 8$.

Figure 12b shows a corresponding assessment of the effect of vertical inhomogeneity on the derived values of effective radius. Since the effective radius is known to increase with increasing height in clouds (cf. Fig. 11), it is to be expected that the derived value of r_{remote} should be less than r_t and greater than r_b, but what radius or altitude level does r_{remote} correspond to? Figure 12b shows r_{remote}/r_t as a function of τ_c and r_t for inhomogeneous models A and B. These results show that r_{remote} is typically 85%–95% of r_t for model A (72%–90% for model B). Furthermore, this figure shows that r_{remote} approaches r_t as the cloud optical thickness increases. The variability in the derived values of r_{remote}/r_t, illustrated in Fig. 12b as error bars displaced from their corresponding mean values at $r_t = 8\ \mu$m, is generally comparable to the uncertainty arising from various values of r_t. In general, we conclude that the retrieved value of r_{remote} depends primarily on τ_c and the inhomogeneous model, with a negligible dependence on the effective radius at cloud top. Since all results presented in Fig. 12 were obtained by applying the two channel algorithm (0.75 and 2.16 μm) to our simulated measurements, the values of $r_{\text{remote}} \geq r_t$ shown in Fig. 12b arise from our algorithm selecting the larger of the two possible radii solutions, rather than the smaller (correct) solution. This multivalued solution can be

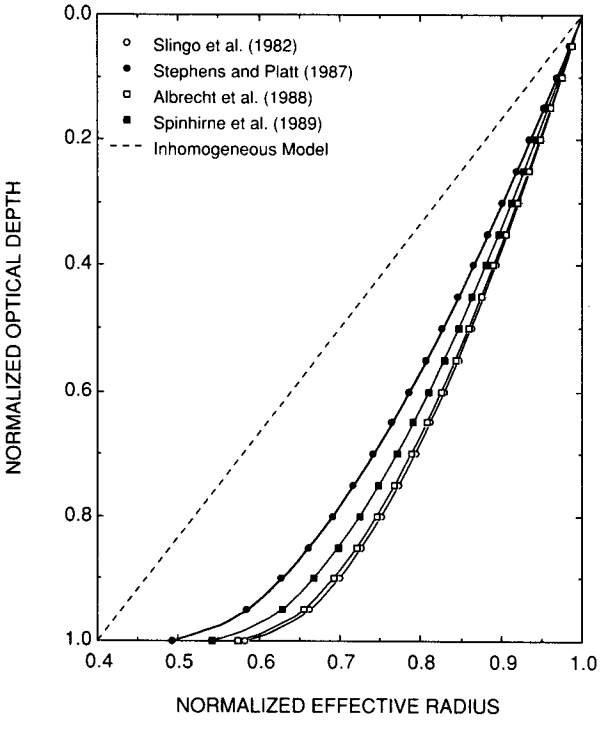

FIG. 11. Normalized effective radius as a function of normalized optical depth. The solid curves and data points were derived from measurements in marine stratocumulus clouds. The Albrecht et al. (1988) profile (open squares, model A) and hypothetical inhomogeneous model (dashed line, model B) were used to simulate the effects of vertical inhomogeneity on the retrieval of cloud optical thickness and effective radius.

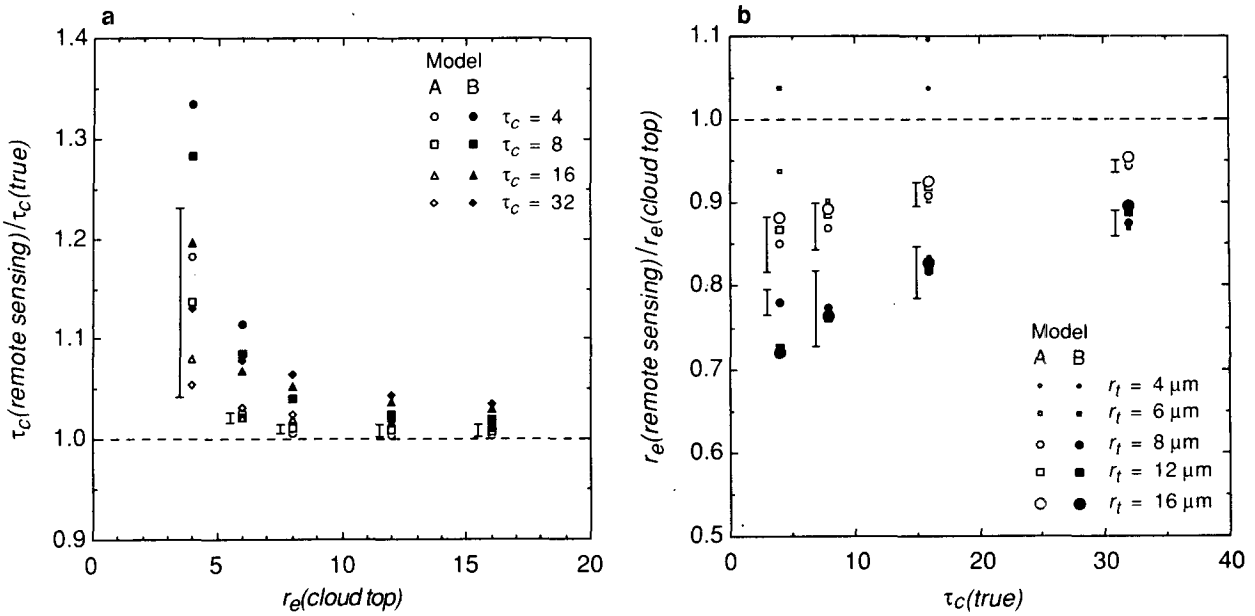

FIG. 12. Ratio of the (a) remote sensing-derived cloud optical thickness to the true optical thickness and (b) remote sensing-derived effective radius to the effective radius at cloud top as a function of r_t and τ_c for two vertically inhomogeneous cloud models.

eliminated by using multiple wavelengths, as discussed in section 4 (cf. Fig. 8).

A careful examination of Figs. 12b and 11 reveals that our remote sensing method is sensitive primarily to the effective radius at some optical depth τ_{eq} within the cloud layer, with little sensitivity to the inhomogeneous model. For example, when $\tau_c = 16$ and inhomogeneous model A applies, $r_{remote} \approx 0.91 r_t$, which corresponds to $\tau_{eq} \approx 0.33\tau_c$. In contrast, $r_{remote} \approx 0.82 r_t$ and $\tau_{eq} \approx 0.30\tau_c$ for model B, thereby suggesting that $\hat{\tau}_{eq}$ is the parameter that is the most similar for various degrees of vertical inhomogeneity.

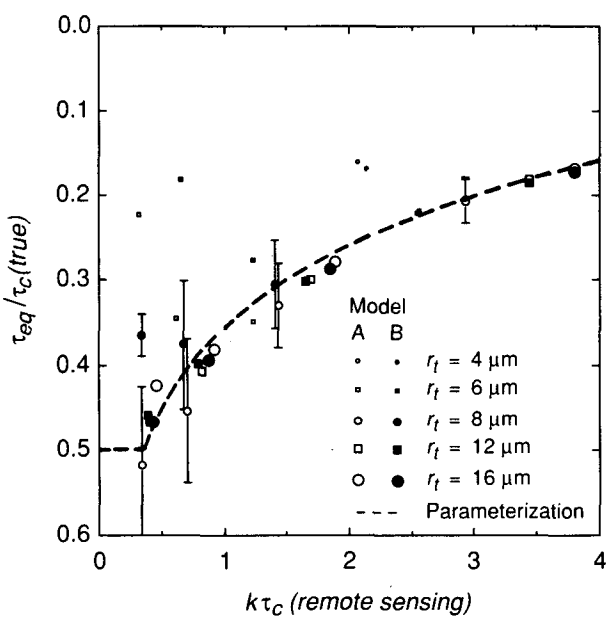

FIG. 13. Normalized equivalent optical depth $\hat{\tau}_{eq}$ as a function of $k\tau_c$, where k is the diffusion exponent at 2.16 μm and both k and τ_c are derivable from remote sensing-derived values of cloud optical thickness and effective radius. The parameterization curve is used to determine the optical depth level within the cloud for which the derived effective droplet radius applies.

Figure 13 illustrates $\hat{\tau}_{eq}$ as a function of $k\tau_{remote}$, where k is the diffusion exponent at 2.16 μm, a function of effective radius r_{remote}. This choice of variable was suggested by the asymptotic expression for the reflection function of thick atmospheres [Eq. (4)], since $k\tau_c$ enters the expression and not τ_c alone. From the computational results presented in Table 1, k can be approximated as:

$$k = 4.92 \times 10^{-3} + 4.04 \times 10^{-2} \ln(r_e). \quad (24)$$

A similar parameterization can easily be developed for other wavelengths such as 3.70 μm.

The results presented in Fig. 13 show that as either the cloud optical thickness or diffusion exponent increases, the effective radius inferred from reflected solar radiation measurements is sensitive to higher levels within the cloud. When using 2.16 μm to infer the effective radius, r_{remote} corresponds to an optical depth 20%–40% of the total optical thickness of the cloud layer. These simulations lead to the following simple parameterization:

$$\hat{\tau}_{eq} = \min(0.365 - 0.145 \ln(k\tau_c), 0.5), \quad (25)$$

illustrated in Fig. 13 as a dashed line.

In order to be applicable to the problem of determining the effective radius at cloud top or some arbitrary level within the cloud, the remote sensing values of τ_{remote} and r_{remote} can be used to determine the abscissa values of $k\tau_c$ in Fig. 13 and applied to Eq. (25). Thus our approach can be summarized as follows:

(i) Determine τ_{remote} and r_{remote} assuming a vertically homogeneous atmosphere, as outlined in section 4.

(ii) Calculate k using Eq. (24), with $r_e = r_{\text{remote}}$.

(iii) Determine $\hat{\tau}_{\text{eq}}$ from Eq. (25), where $k\tau_c = k\tau_{\text{remote}}$.

(iv) Determine $\hat{r}_{\text{remote}}$ assuming an inhomogeneous vertical stratification such as Albrecht et al.'s (1988) model for which $\hat{r}_b = 0.57$ [Eqs. (21) and (22)].

(v) Adjust the retrieved value of r_{remote} to determine the effective radius at cloud top (r_t) or some arbitrary level within the cloud using Eq. (21).

Thus, if we obtain $\tau_{\text{remote}} = 10$ and $r_{\text{remote}} = 8$ μm using the two channel algorithm based on measurements $R^{0.75}_{\text{meas}}$ and $R^{2.16}_{\text{meas}}$, we obtain $\hat{\tau}_{\text{eq}} = 0.38$, which further suggests that the remotely sensed effective radius is 90% of the cloud top value for the Albrecht et al. model of marine stratocumulus clouds. At 3.70 μm, the effective radius derived from reflected solar radiation measurements is within 90% of its cloud top value for all $\tau_c \geq 5$.

7. Discussion and concluding remarks

A statistical technique has been developed for inferring optimum values of the optical thickness and effective radius of clouds from multiwavelength reflected solar radiation measurements. The procedure incorporates a new discrete ordinates radiative transfer method as well as asymptotic expressions for the reflection function of optically thick layers, thereby permitting accurate reflection function tables to be computed efficiently. Since asymptotic expressions for the reflection function are valid to an accuracy of better than 1% for scaled optical thicknesses ≥ 1.5 (optical thicknesses ≥ 9), these analytic expressions can be used to analyze reflected solar radiation measurements when the clouds are optically thick. The use of asymptotic theory significantly reduces the number of interpolations and thereby the computer time required to analyze scenes containing optically thick pixels. Such fast yet accurate algorithms are especially useful for analyzing two-dimensional satellite images. In spite of these advantages, our method is still based on plane-parallel geometry and may thus prove unsatisfactory for clouds with vertical boundaries.

As illustrated by the family of curves in Figs. 2 and 7, the information content of reflection function measurements at 0.75 and 2.16 μm is nearly orthogonal for optically thick layers. These computations demonstrate that the reflection function at 0.75 μm is primarily sensitive to cloud optical thickness [τ_c (0.75 μm)], whereas the reflection function at 2.16 μm is primarily sensitive to effective droplet radius (r_e). When the cloud optical thickness is small an ambiguity arises in determing r_e, due primarily to the fact that the scaled optical thickness is greater at 2.16 μm than at 0.75 μm, with the greatest enhancement occurring when $r_e \approx 5$ μm. Under these conditions a two-channel algorithm based on reflectance measurements at 0.75 and 2.16 μm alone can lead to multiple solutions for r_e and τ_c (0.75 μm).

Our numerical simulations have shown that a third channel near 1.65 μm does not substantially improve the retrieval for liquid water clouds. Furthermore, the magnitude of the minimum value of the statistic χ^2, defined by Eq. (11) and illustrated in Fig. 8, is not a sufficient index for assessing the soundness of the retrieval. In order to eliminate multiple solutions from occurring for small values of τ_c (0.75 μm) and r_e, it is preferable to use results obtained from several sets of wavelengths or to make use of reflectance measurements around 3.70 μm. The 3.70 μm measurements are especially useful but must be corrected for thermal emission, which also contributes to the upwelling intensity at this wavelength. Other than in these multiple solution cases, the two channel method is adequate for estimating τ_c (0.75 μm) and r_e.

Uncertainties in the cloud optical thickness and effective radius arising from 5% measurement errors are assessed in Figs. 9 and 10. Figure 9, which is based on simulations of the spherical albedo, represents mean uncertainties for a range of solar zenith angles and observational zenith and azimuth angles, and would be somewhat reduced for small solar zenith angles with forward scattering, and somewhat enhanced for large solar zenith angles with backward scattering. Figure 6 shows, for example, that the simultaneous determination of τ_c (0.75 μm) and r_e is especially difficult in the backscattering direction.

The results presented in Fig. 7 suggest that τ_c (0.75 μm) and r_e can be determined for aerosol layers using exactly the same technique as that proposed here for clouds, since the information content of the reflection function at 0.75 and 2.16 μm is once again orthogonal in τ_c (0.75 μm) and r_e for optically thin layers. In order to apply this technique to cloud-free scenes, however, it is necessary to have a good estimate of the dispersion of the aerosol size distribution σ and the ground reflectivity A_g. Kaufman et al. (1990) use essentially this technique to derive the aerosol optical thickness and particle size from NOAA/AVHRR images.

Finally, we have investigated the effect of vertical inhomogeneity on the retrieval of cloud optical thickness and effective radius. Our simulations suggest that it is sufficient to assume a vertically homogeneous cloud layer when interpreting experimental observations, and

that the derived optical thickness differs from the true optical thickness by no more than 3% for typical inhomogeneous conditions. The effective radius retrieval, on the other hand, represents an effective radius at an equivalent optical depth within the cloud layer, and is typically 85%–95% of the radius at cloud top. As the effective radius at cloud base is approximately 57% of that at cloud top, we conclude that the effective radius retrieved from our analysis represent the effective radius at an optical depth 20%–40% of the total optical thickness of the cloud layer. We have developed a parameterization which permits one to adjust the remotely sensed effective radius to an arbitrary level within the cloud, such as the midcloud level where in situ cloud microphysical measurements are often obtained.

In Part II we will present results for the optical thickness and effective radius of clouds derived from measurements of the reflection function obtained using the Multispectral Cloud Radiometer described by Curran et al. (1981) and King (1987). These measurements were obtained from the NASA ER-2 high-altitude aircraft during the marine stratocumulus intensive field observation component of FIRE, conducted off the coast of southern California during July 1987. Finally, these analyses will be compared to in situ microphysical measurements obtained with the University of Washington C-131A aircraft.

Acknowledgments. The authors are grateful to G. T. Arnold and H. G. Meyer for aid in performing the computations. This research was supported by NASA's Climate Program, and was performed while Teruyuki Nakajima held a senior National Research Council Resident Research Associateship in the Laboratory for Atmospheres, Goddard Space Flight Center.

REFERENCES

Albrecht, B. A., D. A. Randall and S. Nicholls, 1988: Observations of marine stratocumulus clouds during FIRE. *Bull. Amer. Meteor. Soc.*, **69,** 618–626.

Arking, A., and J. D. Childs, 1985: Retrieval of cloud cover parameters from multispectral satellite images. *J. Climate Appl. Meteor.*, **24,** 322–333.

Bevington, P. R., 1969: *Data Reduction and Error Analysis for the Physical Sciences.* McGraw-Hill, 336 pp.

Cess, R. D., G. L. Potter, J. P. Blanchet, G. J. Boer, S. J. Ghan, J. T. Kiehl, H. Le Treut, Z. X. Li, X. Z. Liang, J. F. B. Mitchell, J. J. Morcrette, D. A Randall, M. R. Riches, E. Roeckner, U. Schlese, A. Slingo, K. E. Taylor, W. M. Washington, R. T. Wetherald and I. Yagai, 1989: Interpretation of cloud-climate feedback as produced by 14 atmospheric general circulation models. *Science,* **245,** 513–516.

Charlson, R. J., J. E. Lovelock, M. O. Andreae and S. G. Warren, 1987: Oceanic phytoplankton, atmospheric sulphur, cloud albedo and climate. *Nature,* **326,** 655–661.

Cline, A. K., 1974: Scalar- and planar-valued curve fitting using splines under tension. *Assoc. Comput. Mach. Commun.*, **17,** 218–220.

Coakley, J. A., Jr., R. L. Bernstein and P. A. Durkee, 1987: Effect of ship-stack effluents on cloud reflectivity. *Science,* **237,** 1020–1022.

Curran, R. J., and M. L. C. Wu, 1982: Skylab near-infrared observations of clouds indicating supercooled liquid water droplets. *J. Atmos. Sci.*, **39,** 635–647.

——, H. L. Kyle, L. R. Blaine, J. Smith and T. D. Clem, 1981: Multichannel scanning radiometer for remote sensing cloud physical parameters. *Rev. Sci. Instrum.*, **52,** 1546–1555.

Durkee, P. A., 1989: Observations of aerosol-cloud interactions in satellite-detected visible and near-infrared radiance. *Proc. Symp. on the Role of Clouds in Atmospheric Chemistry and Global Climate,* Amer. Meteor. Soc., Anaheim, 157–160.

Foot, J. S., 1988: Some observations of the optical properties of clouds. I: Stratocumulus. *Quart. J. Roy. Meteor. Soc.*, **114,** 129–144.

Hansen, J. E., and J. B. Pollack, 1970: Near-infrared light scattering by terrestrial clouds. *J. Atmos. Sci.*, **27,** 265–281.

——, and L. D. Travis, 1974: Light scattering in planetary atmospheres. *Space Sci. Rev.*, **16,** 527–610.

Hudson, J. G., 1983: Effects of CCN concentrations on stratus clouds. *J. Atmos. Sci.*, **40,** 480–486.

Kaufman, Y. J., R. S. Fraser and R. A. Ferrare, 1990: Satellite measurements of large-scale air pollution—Method. *J. Geophys. Res.*, in press.

King, M. D., 1981: A method for determining the single scattering albedo of clouds through observation of the internal scattered radiation field. *J. Atmos. Sci.*, **38,** 2031–2044.

——, 1987: Determination of the scaled optical thickness of clouds from reflected solar radiation measurements. *J. Atmos. Sci.*, **44,** 1734–1751.

——, L. F. Radke and P. V. Hobbs, 1990: Determination of the spectral absorption of solar radiation by marine stratocumulus clouds from airborne measurements within clouds. *J. Atmos. Sci.*, **47,** 894–907.

Mitchell, J. F. B., C. A. Senior and W. J. Ingram, 1989: CO_2 and climate: A missing feedback? *Nature,* **341,** 132–134.

Nakajima, T., and M. Tanaka, 1988: Algorithms for radiative intensity calculations in moderately thick atmospheres using a truncation approximation. *J. Quant. Spectrosc. Radiat. Transfer,* **40,** 51–69.

Radke, L. F., J. A. Coakley, Jr. and M. D. King, 1989: Direct and remote sensing observations of the effects of ships on clouds. *Science,* **246,** 1146–1149.

Ramanathan, V., 1987: The role of earth radiation budget studies in climate and general circulation research. *J. Geophys. Res.*, **92,** 4075–4095.

——, B. R. Barkstrom and E. F. Harrison, 1989a: Climate and the earth's radiation budget. *Phys. Today,* **42,** 22–32.

——, R. D. Cess, E. F. Harrison, P. Minnis, B. R. Barkstrom, E. Ahmad and D. Hartmann, 1989b: Cloud-radiative forcing and climate: Results from the Earth Radiation Budget Experiment. *Science,* **243,** 57–63.

Roeckner, E., U. Schlese, J. Biercamp and P. Loewe, 1987: Cloud optical depth feedbacks and climate modelling. *Nature,* **329,** 138–140.

Rossow, W. B., L. C. Gardner and A. A. Lacis, 1989: Global, seasonal cloud variations from satellite radiance measurements. Part I: Sensitivity of analysis. *J. Climate,* **2,** 419–458.

——, F. Mosher, E. Kinsella, A. Arking, M. Desbois, E. Harrison, P. Minnis, E. Ruprecht, G. Sèze, C. Simmer and E. Smith, 1985: ISCCP cloud algorithm intercomparison. *J. Appl. Meteor.*, **24,** 877–903.

Salomonson, V. V., W. L. Barnes, P. W. Maymon, H. E. Montgomery and H. Ostrow, 1989: MODIS: Advanced facility instrument for studies of the Earth as a system. *IEEE Trans. Geosci. Remote Sens.*, **27,** 145–153.

Slingo, A., 1989: A GCM parameterization for the shortwave radiative properties of water clouds. *J. Atmos. Sci.*, **46,** 1419–1427.

——, S. Nicholls and J. Schmetz, 1982: Aircraft observations of marine stratocumulus during JASIN. *Quart. J. Roy. Meteor. Soc.*, **108,** 833–856.

Spinhirne, J. D., R. Boers and W. D. Hart, 1989: Cloud top liquid

water from lidar observations of marine statocumulus. *J. Appl. Meteor.*, **28,** 81–90.

Stephens, G. L., and C. M. R. Platt, 1987: Aircraft observations of the radiative and microphysical properties of stratocumulus and cumulus cloud fields. *J. Climate Appl. Meteor.*, **26,** 1243–1269.

Twomey, S., 1980: Cloud nucleation in the atmosphere and the influence of nucleus concentration levels in atmospheric physics. *J. Phys. Chem.*, **84,** 1459–1463.

——, and C. F. Bohren, 1980: Simple approximations for calculations of absorption in clouds. *J. Atmos. Sci.*, **37,** 2086–2094.

——, and K. J. Seton, 1980: Inferences of gross microphysical properties of clouds from spectral reflectance measurements. *J. Atmos. Sci.*, **37,** 1065–1069.

——, and T. Cocks, 1982: Spectral reflectance of clouds in the near-infrared: Comparison of measurements and calculations. *J. Meteor. Soc. Japan,* **60,** 583–592.

——, and ——, 1989: Remote sensing of cloud parameters from spectral reflectance in the near-infrared. *Beitr. Phys. Atmos.*, **62,** 172–179.

——, M. Piepgrass and T. L. Wolfe, 1984: An assessment of the impact of pollution on global cloud albedo. *Tellus,* **36,** 356–366.

van de Hulst, H. C., 1974: The spherical albedo of a planet covered with a homogeneous cloud layer. *Astron. Astrophys.*, **35,** 209–214.

——, 1980: *Multiple Light Scattering. Tables, Formulas, and Applications,* Vols. 1 and 2, Academic Press, 739 pp.

Wetherald, R. T., and S. Manabe, 1988: Cloud feedback processes in a general circulation model. *J. Atmos. Sci.*, **45,** 1397–1415.

Wielicki, B. A., J. T. Suttles, A. J. Heymsfield, R. M. Welch, J. D. Spinhirne, M. L. C. Wu, D. O'C Starr, L. Parker and R. F. Arduini, 1990: The 27–28 October 1986 FIRE IFO Cirrus case study: Comparison of radiative transfer theory with observations by satellite and aircraft. *Mon. Wea. Rev.*, in press.

Wigley, T. M. L., 1989: Possible climate change due to SO_2-derived cloud condensation nuclei. *Nature,* **339,** 355–357.

Wu, M. L., 1985: Remote sensing measurements of cloud physical parameters in the cooperative convective precipitation experiment. *J. Geophys. Res.*, **90,** 10 551–10 562.